Desalination and Water Treatment
www.deswater.com
doi: 10.5004/dwt.2023.29672

298 (2023) 1–11
June

Biological and corrosion aspects of a multi-stage flash seawater desalination plant after deaerator modification

Troy N. Green[a,*], Ali A. Al-Sahary[a], Friedrich Alt[a], Christopher M. Fellows[a,b], Nikolay Voutchkov[c], Abdurrahman Alenazi[a]

[a]*SWCC: Desalination Technologies Research Institute (DTRI), Saudi Arabia, Tel.: +96613 3430333 Ext. 31715; email: Tgreen@swcc.gov.sa (T.N. Green), Tel.: +96613 3430333 Ext. 31779; email: Aal-Sahary@swcc.gov.sa (A.A. Al-Sahary), Tel.: +96613 3430333 Ext. 31705; email: Falt@swcc.gov.sa (F. Alt), Tel.: +46 730472263; email: CMichael@swcc.gov.sa (C.M. Fellows), Tel.: +96613 3430333 Ext. 31781; email: AAlenazi5@swcc.gov.sa (A. Alenazi)*
[b]*The University of New England: School of Science and Technology, Australia*
[c]*ENOWA Water Innovation Center, Saudi Arabia, Tel.: +96612 32531312; email: Nikolay.voutchkov@neom.com*

Received 13 March 2023; Accepted 30 May 2023

ABSTRACT

Deaeration units of a commercial multi-stage flash (MSF) cogeneration facility underwent venting modifications to increase system distillate productivity without increasing energy consumption or elevating top brine temperatures. Three MSF units were investigated after oxygen levels of deaerators spiked above design limits (20 ppb). The investigation found a significant biotic presence in the deaerator unit's MSF heat rejection sections that included algae, bacteria, bivalves, and bivalve larvae. The bivalve taxa consists of *Barbatia parva*, *Diodora funiculata*, *Pinctada margaritifera*, *Amiantis umbonella*, and *Acrostergma assimile*. Galvanic corrosion exacerbated by biofilm was also observed in heat rejection sections. While attesting to the tenacity and adaptability of marine life, the presence of biological communities is symptomatic of the abnormally high oxygen levels in deaerator units. Elevated oxygen levels contribute to systems performance declines resulting from biological fouling of deaerator packing materials, partially responsible for inefficiencies in reducing the gas solubilities of MSF process feed waters and elevated concertation ratios [1,2]. Several thermal desalination units presented similar process issues, but one was selected for detailed inspection and evaluation.

Keywords: Multi-stage flash; Microbial corrosion; Rubber devulcanization; Deaerator

1. Introduction

The purging of non-condensable gases – in a vacuum system is best articulated by Henry's Law, relating system pressure decrease to decreased solubility, and inverse solubility law relating temperature increase to decreased solubility. Steam in deaerator systems lowers the partial pressure and increases the temperature, reducing the solubility of gases in the make-up feed water. At atmospheric pressure and 25°C, expected concentrations in water at equilibrium with air are 8 parts per million (ppm) O_2, 14 ppm N_2, and 0.5 ppm CO_2. At 0.7 bar and 90°C, these concentrations should reduce to 1 ppm O_2, 2 ppm N_2, and 0.01 ppm CO_2 – with the difference amounting to 30 dm^3 of gas per m^3 of brine [3].

In thermal multi-stage flash (MSF) systems, the optimum release of non-condensable gases (nitrogen, oxygen, and carbon dioxide) from system feed water and concentrated brine in flash chambers is critical for controlling corrosion and alkaline scale formations [1]. Nitrogen is inert and mostly non-reactive with elements, compounds, and

* Corresponding author.

metals. Nitrogen degassing effects on metal corrosion indirectly result from a pH drop, which can gradually degrade the oxide layer, exposing the metal to a corrosive solvent. In contrast, oxygen and carbon dioxide are very reactive and can react directly with metal oxide and metal, promoting corrosion.

Metal exposure to oxygen encourages metal oxidation (metal oxide formation) which, over time, weakens metals. Oxygen degassing also can promote corrosion by disrupting the metal oxide in the oxygen due to the decreased concentration gradient from oxygen purging – exposing the metal to the corrosive environment of the solvent.

CO_2 corrosion results from the formation of carbonic acid, which can attack the metal surface and is more likely to happen in the presence of chloride. CO_2 in a solution can also positively produce a passivating layer on the surface of metals. The degassing of CO_2 can decrease carbonic acid levels and increase pH but may remove the coating from carbonate on the metal, exposing the metal to the corrosive environment of the solvent. In the presence of organic materials (foulants [microbes, biochemical polymers, etc.]), an inefficient purge of non-condensable gases can cause tube sections' blanketing, producing heat transfer resistance (similar to the design fouling resistance), decreasing system efficiency, increasing energy consumption [2] and promote fouling of deaerator pall rings and structures. Due to elevated oxygen saturation levels, investigations of the deaerator and other parts of MSF units were conducted.

The deaerator units investigated are part of a cogeneration (power-potable water production) desalination plant in the Eastern Province of Saudi Arabia (Fig. 1). One of seven desalination units (each containing 23-stage flash chambers) was chosen for a detailed inspection. At the time of examination, units had been operating for 65 months (since commissioning) with 25 months of continuous operation (since their last shutdown).

The inspection focussed on biological and material degradation aspects of the; deaerator, heat rejection section (units 21, 22, and 23), and heat recovery sections, including water boxes, flash chambers, and the brine heater.

2. Deaerators

Six deaerator units were examined before their online oxygen measuring systems were calibrated. All units were checked and calibrated with the Orbisphere 3100 portable oxygen saturation device and displayed oxygen concentrations above 20 parts per billion (ppb) – the maximum saturation design limit (Fig. 2). Elevated oxygen concentrations were indicative of a system defect requiring shutdown and inspection.

After the initial inspection and calibration, system modifications were done in two deaerators (73 and 76) to enhance production by closing the middle vent outlets for non-condensable gases. The primary aim of this study was to examine the effects of the deaerator's modifications. Units 73 and 76 (test units) were compared with control units (71, 72, 74, 75, and 78) after 18,000 h of operation. High oxygen levels of control and test units confirm that elevated values are not due to system modifications. However, as the systems are designed to achieve an oxygen saturation below 20 ppb, biofouling of the deaerator and polypropylene

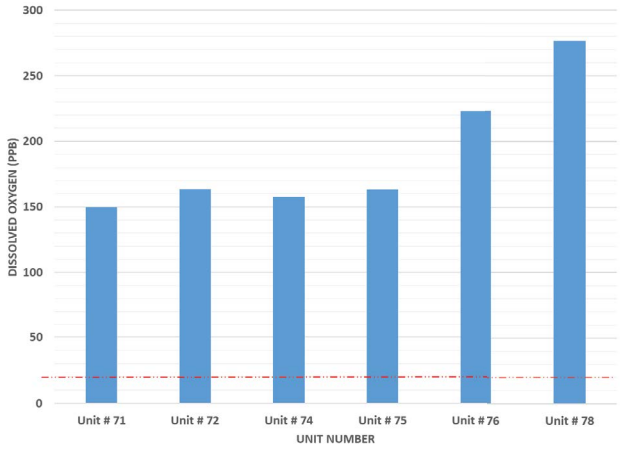

Fig. 2. Dissolved oxygen measurements of different units within the plant.

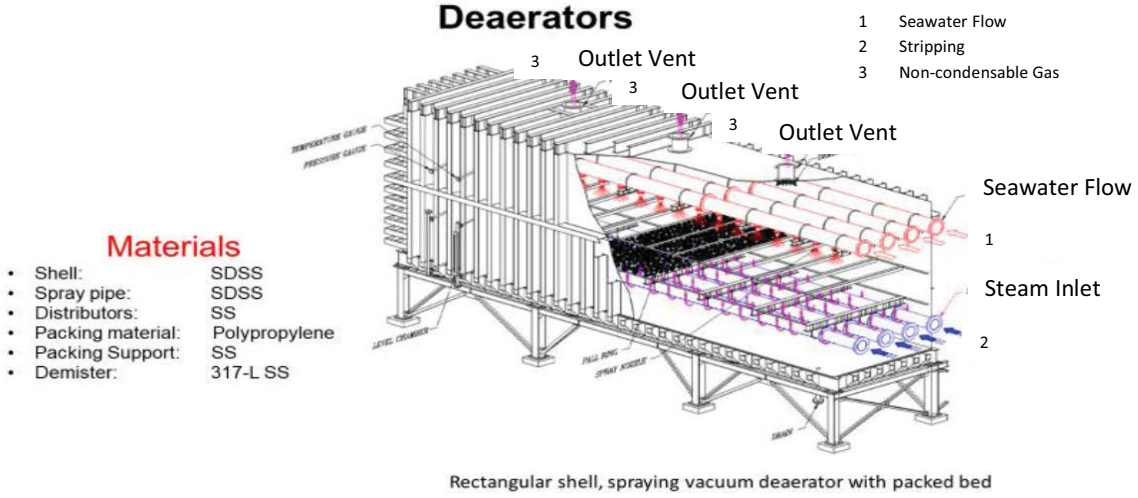

Fig. 1. A deaerator unit with inspection demarcations (cogeneration desalination unit).

pall ring packing materials are suspected to be the reason for the deaerators declining performance.

Cascade beta-rings (pall rings) or other component fouling within the deaerator packing material can cause inefficient droplet dispersions of the sprayed make-up feed water, impacting heat saturation levels from steam designed to liberate non-condensable gases (Fig. 1). Packing material fouling can result from upstream biological fouling of feed lines or increased organic load in the make-up feed water, enhancing deposition and biological fouling on pall rings. A plant shutdown and systems inspection order was given to investigate the cause and impact of high oxygen saturation in deaerators.

3. Methodology

Seawater was evacuated from the seven MSF units (five control units [71, 72, 74, 75 and 78] and two tests [73 and 76]), ventilating all chambers. Visual inspection was the primary technique for observing material differences before and after system modifications. Inspections were conducted on deaerators and in heat-rejection, heat-recovery, and series flash chambers. Test MSF units 73 and 76 were similar in production and performance; therefore, unit 73 was selected for more detailed inspections and analyses.

Sludge was collected from the bottom of the deaerator unit and around underneath the gasket of the manhole. Samples were assayed for organic and inorganic content using loss of initiation, scanning electron microscopy/energy-dispersive X-ray spectroscopy (SEM/EDX), X-ray diffraction (XRD), and microscopic analyses.

For loss of ignition tests, samples were collected and dried in a desiccator, weighed (up to 5 g) in a crucible, transferred to a preheated furnace 550°C ± 25°C, and burned for 30 min. Samples were cooled in a desiccator, weighted, and the dry mass's ignition loss was calculated (European Standard TC-WI 2003[E]).

SEM/EDX analysis samples were series dehydrated with 10%, 20%, 30%, 50%, and 80% isopropanol attached to double-sided conductive carbon tape slugs and then platinum-coated (JEOL JFC-1100E iron-sputtering device, Japan). Samples were examined at an acceleration voltage of 20kV.

XRD (Rigaku MiniFlex) was used to identify minerals in samples. Excess dehydrated samples prepared for SEM were used for non-destructive XRD (X-ray generator [40 kV, 15 mA], scan speed 5.00°/min, scan axis θ/2, and scan range 3°~90°).

Shells and sand-like materials were collected from deaerators, and the heat rejection sections and identified. The Nikon Eclipse Ci multi-magnifier light microscope (H550-S) with Y-V TV was used to identify micro bivalves, bacteria, detritus, and diatomaceous material. In addition, a MiniFlex 600 with Cu tube, 40 kV, with a scan range of 3°–90°, was used to characterize deposits.

4. Results and discussion

4.1. Modified deaerator unit [unit 73] inspection

4.1.1. Lower area

The area of the deaerator beneath the packing material contained sand with black particulates (Fig. 3). Balls from the ball cleaning system were also found. In addition, noticeable reddish streaks were observed on metal steam lines at the base of the packing support structure and struts holding steam lines – presumably due to iron oxide formations.

4.1.2. Maintenance hole door

Samples of material obtained from beneath the gasket attached to the maintenance hole door appear to contain sulfur and iron (Fig. 4) – confirmed by SEM/EDX. In addition, high percentages of magnesium, carbon, and oxygen are observed (Fig. 4), in addition to trace concentrations of aluminum and silica.

Iron and magnesium can indicate corrosion products in the form of oxides, which also suggests the presence of oxygen oxidation in the deaeration feed water. In the EDX results, sulfur is also observed, explaining rubber vulcanization's faint but pungent smell [4]. Gasket performance failure is most prominent at the bottom of the manhole door (Fig. 4). Improper gasket sealing around the maintenance hole results in air leakage, vacuum losses, and system performance reduction. Material biodegradation is suspected to be a cause of the mechanical seal (gasket) detachment. Copious amounts of slime material were observed under the gasket's areas, and high carbon and oxygen ratios (SEM/

Fig. 3. Lower area of deaerator (unit 73).

EDX) confirmed biofilm presence (Fig. 4). Silica is most likely associated with sand (in the deaerator system) and diatomaceous material (Figs. 5 and 6).

4.1.3. Manhole entrance

Copious amounts of sludge comprised of organic and diatomaceous materials were found at the bottom of the deaerator (Fig. 5), as confirmed by microscopic. A significant portion of a black substance (with a distinct H_2S smell) under the top layer of the sludge contained sulfur-reducing bacteria (BART-SRB test) and iron related bacteria (BART-IRB test), respectively (Fig. 6).

Deposits collected from the maintenance hole door and entrance to the deaerator contain iron deposits, organic material, diatomaceous matter, and microbes. Bivalve larvae were the dominant biota (by size) under microscopic examination (Fig. 7). Bacterial isolates were rod and cocci shaped with ciliated movements.

XRD analysis of inorganic samples from the maintenance hole entrance indicates the presence of aragonite (Fig. 8) and a large proportion of poorly resolved amorphous material (Fig. 8). Aragonite and the high magnesium content from EDX analysis (Fig. 4) are consistent with bivalve biomineralized aragonite production [5]. The absence of sharp peaks is likely due to organic presence within the sample (though samples were cleaned, aspirated, and sequence dehydrated with isopropanol [Fig. 8]).

Microscopic analysis revealed that samples from the top of the deaerator manhole entrance (Fig. 6) contained bacterial and filamentous algae as part of the biomatrix (Fig. 9). However, zooplankton species that do not manufacture biofilm were not observed – consistent with chlorination pre-treatment where bivalves and bivalve larvae thrive exclusively on biochemically vulnerable planktonic species.

4.2. Top area of the deaerator (vapour side-space above the packing material)

Above the packing material, at the top of the deaerator, the scale fouling was smooth, solid, and adherent, extending above the waterline towards the roof of the deaerator near spray nozzles without signs of biofouling or corrosion.

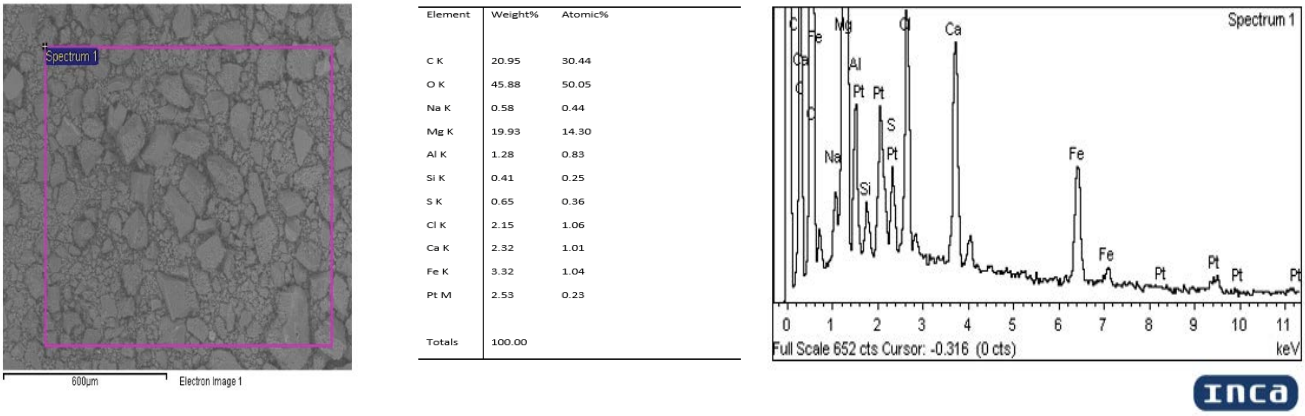

Fig. 4. Scanning electron microscopy/energy-dispersive X-ray spectroscopy results for samples collected under the gasket of the deaerator manhole.

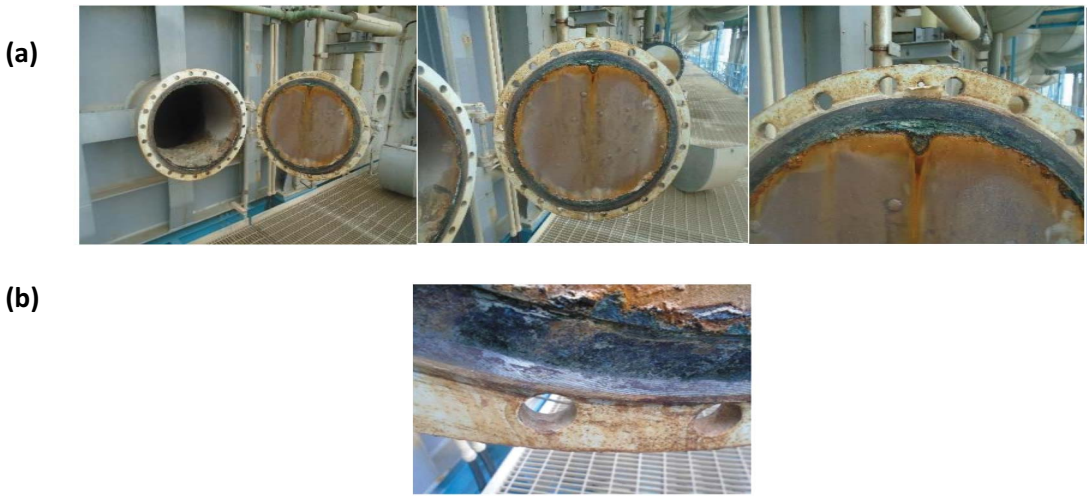

Fig. 5. Lower maintenance hole door of unit 71 (a) with gasket and (b) without gasket.

Some surface oxidation was noticed on the interior near the maintenance hole door without indicating signs of metal oxidation (Fig. 10).

XRD of the hard scale observed on the vapor side of the deaerator contained aragonite – the thermodynamically favorable form of calcium carbonate (Fig. 11).

Fig. 6. Deposits on the maintenance hole door, manhole entrance, and inside of the multi-stage flash deaerator.

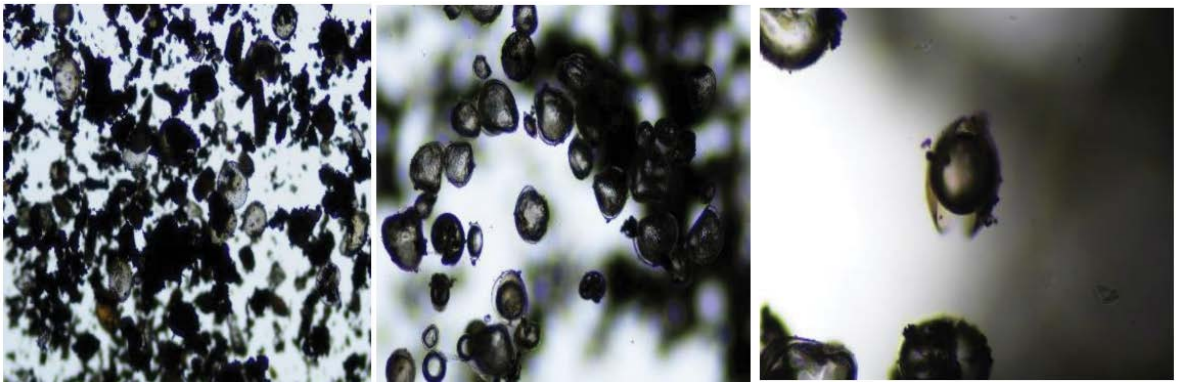

Fig. 7. Microscopic profile of species extracted from the manhole door, entrance, and inside of the deaerator (predominance of bivalve larvae).

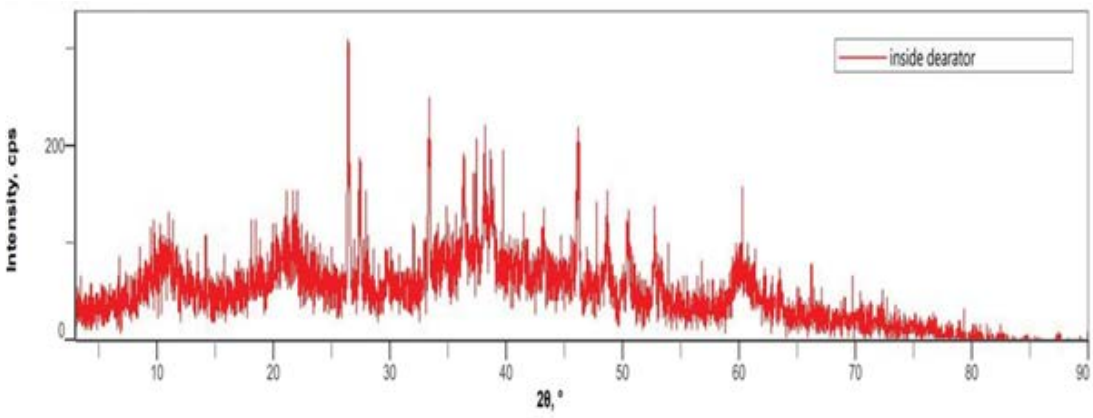

Fig. 8. X-ray diffraction analysis of inorganic samples from the deaerator manhole entrance.

4.2.1. Heat rejection section

Large numbers of viable, mature bivalves were observed in the area where the cooling water discharges from the heat rejection system – after traveling through tube bundles of stages 23, 22, and 21 (Fig. 12). *Barbatia parva*, *Diodora funiculata*, *Pinctada margaritifera*, *Amiantis umbonella*, and *Acrostergma assimile* were observed. The ages of bivalves are estimated at between six months and 2 y – taking into account the combined theories of Kleiber [6], Kooijman [7], and Peters [8]. The location of these shells covering the separation grate can promote seawater degassing, producing pressurized zones within the system resulting in mechanical stress on glass fiber reinforced polymer – resulting in delamination, leaks, and cracks (Fig. 13).

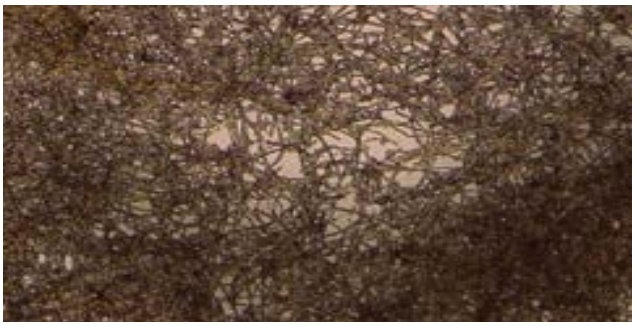

Fig. 9. Filamentous algae from the biomatrix of samples from the top of the manhole entrance.

The presence of bivalve larvae and mature bivalves within the MSF process also raises concern for heat exchanger tubes in the early stages of the heat recovery system, where temperatures are suitable for biological growth, metabolism, and fouling (between 25°C–38°C). In the hotter portions of the heat recovery system, where conditions are lethal to macro and microorganisms, an increase in inorganic and degraded organics in the seawater feed from chemical and thermal degradation of plankton and crustaceans can have an impact on increased organic alkalinity and nucleation and growth of scale on flash chambers and heat exchange structures [9,10].

Fig. 10. Deaerator above the packing – manhole entrance and internal compartment.

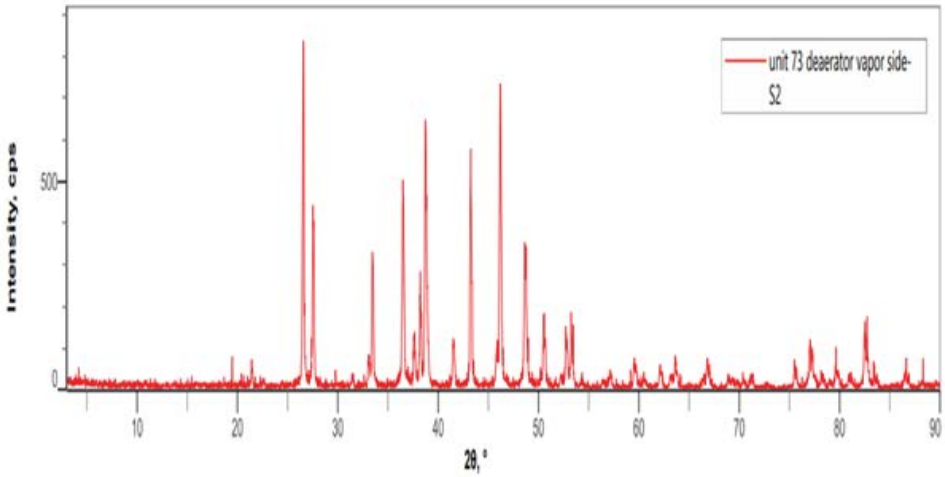

Fig. 11. X-ray diffraction of deaerator scale from the vapor side above the packing material.

4.3. Heat rejection section (crevice-galvanic corrosion/pitting and microbial induced corrosion)

Stage 22 of the heat rejection system experienced crevice corrosion that accelerate galvanic corrosion due to the contact of different metals and the presence of a galvanic couple. Small areas of exposed metal accelerate the corrosion rate from anode/cathode concentration points that promote more electron/proton exchange leading to metal degradation. Upon detailed inspection, pitting corrosion is also observed. Iron-associated bacteria (from the BART IRB test) and microbial biofilms (from microscopic examinations) were present (Fig. 14). Iron-associated bacteria and biofilm suggest the existence of microbially induced corrosion (MIC), which can exacerbate crevice and galvanic corrosion.

4.3.1. Heat rejection section (asbestos gaskets)

Cuts and tares in asbestos gaskets were observed in stages 21 and 22 of the heat rejection section (Fig. 15). The causes of the material failure appear to be an installation defect resulting in water seepage into fibers. Asbestos gaskets are durable and resistant to high temperatures. However, using asbestos gaskets in water treatment systems poses health risks to humans (during installation and replacement) and ecological hazards to aquatic organisms if leached back into seawater. Therefore, industries are increasingly turning to high-performance gaskets made from graphite: clavar, or PTFE, as replacements for asbestos [11].

4.3.2. Heat recovery section (water boxes)

Bivalves ranging in size from 16–19 mm were observed (like Fig. 12) in the heat recovery section of MSF unit 73. However, bivalve sizes were insufficient to clog water box tubes that average 50 mm in diameter. Clogging of lines occurs by several factors that include the dissolution of solid particles from the solution (to heat exchanger tube surfaces) that progressively bind organics, heavy metals and microorganisms, diatoms, and other biomaterials to exchanger

Fig. 12. Mature bivalves at the discharge of heat rejection system of unit 73.

Fig. 13. Glass fiber reinforced polymer damage due to pressurized oxygen build-up from the deaerator feed lines from the heat rejection section of a commercial Arabian Gulf multi-stage flash plant.

tubes. The particulate attachment to heat exchanger tubes promotes surface roughness – further enhancing particle settlement that leads to flow rate drops across heat the pipes, increasing system temperatures, causing scale formations and product water declines, leading to accelerated blockage of lines [12]. Though bivalves may not be enough to clog tubes alone, they can significantly promote pressure drops and the attachment of dissolved inorganic and organic particulates from seawater to heat exchanger tube surfaces, enabling blockage. Settlement fouling can result

Fig. 14. Galvanic and pitting corrosion with microbially induced corrosion.

Fig. 15. Unit 23 asbestos gasket removal and protective paint removal.

in performance declines in pumps, cooling water systems, power generation systems, and thermal desalination systems.

4.3.3. Heat recovery section (flash chambers)

In flash chambers, sand-like material was observed throughout the heat recovery process. The material was collected (from stages 1 and 20) and analyzed using XRD (Fig. 16a and b, respectively).

In stage 1 of the MSF flash chamber, XRD analysis revealed the exclusive presence of brucite (Mg_2 [10] in the 'sand-like material'). Findings are consistent with previous reports of El-Din and Green in their analyses of brucite-containing scale in the early stages of MSF flash chambers [10,12–14]. Brucite can come from biogenic sources (reported from some crust-forming red alga [15,16] and diatoms [17]. Brucite is a known component of biomineralization from coral and aquatic vertebrae. In flash chambers, brucite is formed from low CO_2 and high pH [18] seawaters – consistent with flash chamber conditions and degassing of CO_2.

In stage 20, the site of the coldest brine heater feed water and flash chamber seawater, XRD analysis reveals that the sand-like material on the flash camber surface floor contains aragonite and amorphous deposits. The predominance of aragonite at lower temperatures arises from a combination of thermodynamic and kinetic factors [14,15]. It appears from the purity of the sample that these sand-like particulates are derived from scale formed in situ, unlike the more complex samples isolated from the floor of the deaerator (Figs. 3 and 6).

4.3.4. Heat recovery section (sight glass)

Sight glass damage was observed in some MSF units (unit 76). While there was no sight glass damage in unit 73, algal growth was evident on gaskets around the looking glass of chambers 21 and 22 of the heat rejection system (Fig. 17). Algal growth indicates gasket defects and air seepage into the vacuum system. The presence of light, air leakage, moisture, favorable temperatures, and the rough surface of the gasket (that also contained scale deposits) are ideal conditions for algal growth. To correct the problem of the vacuum leak within the heat recovery section. For unit 73, gasket replacement, repair of the looking glass,

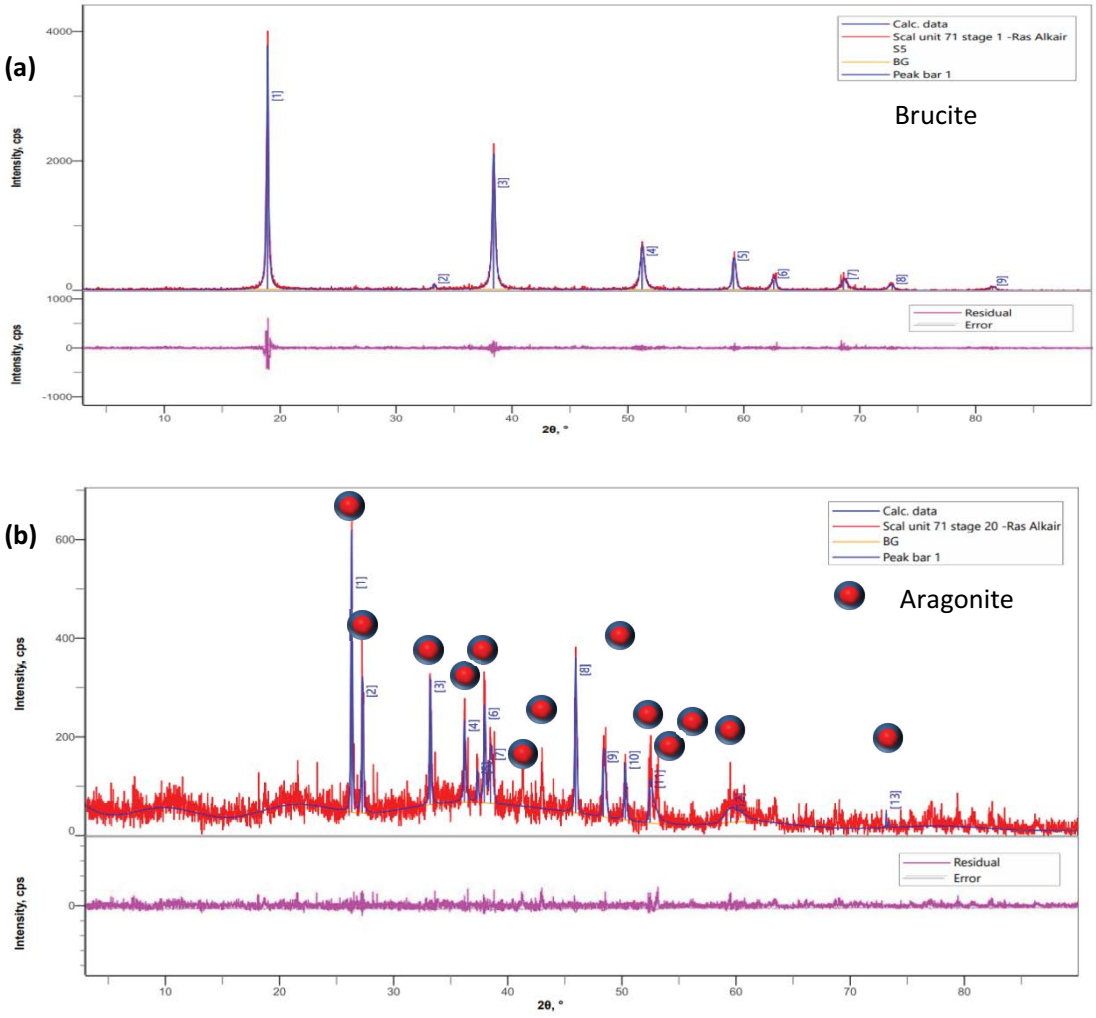

Fig. 16. X-ray diffraction of sand-like material obtained from the floor of (a) stage 1 and (b) stage 20.

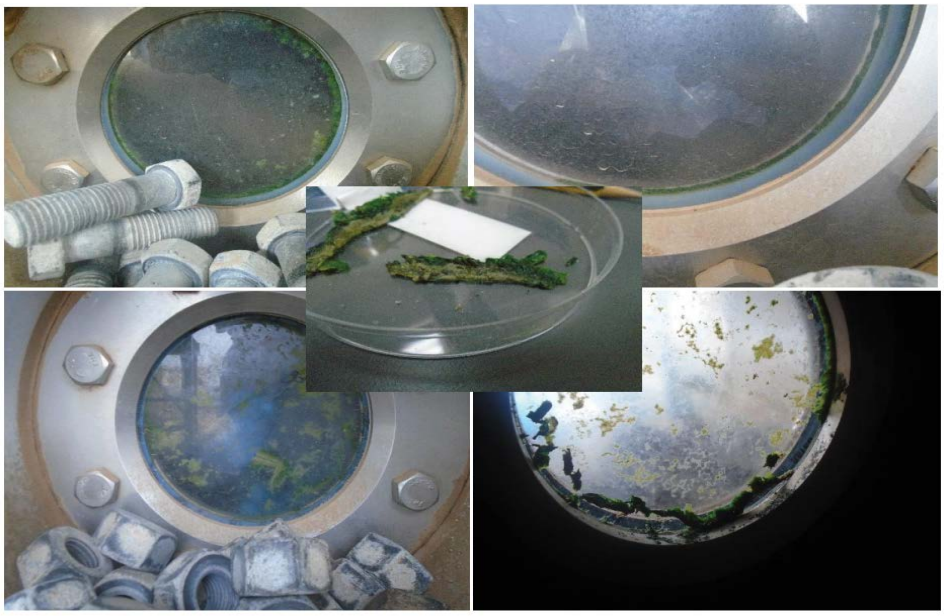

Fig. 17. Multi-stage flash unit 73 looking glasses (chambers 21 and 22).

disinfectant (with DBNPA [a non-oxidative biocide]) followed by a system air leak inspection was recommended. For unit 76, gasket replacement, disinfection, and change of sight glasses followed by a leak test were advised.

4.4. Summary, conclusions, and recommendations

Oxygen concentrations, well above the design limit (>20 ppb), were observed in the deaerators of 6 multi-stage flash units under investigation (71–76 and 78). The previous modification of two units to enhance water production and reduce energy consumption (units 73 and 76) by closing middle vent outlets did not significantly increase oxygen saturation levels compared to control units (71, 72, 74, and 75). Biological fouling of the deaerator packing material and depressurization of the deaerators (due to gasket leaks) is more likely responsible for the inefficiencies in reducing the gas solubility of feed waters in deaerators. Potential system leaks from the heat rejection system's sight glass gaskets, water boxes, and asbestos gaskets require further investigation but may play a role in deaerator depressurization, increased oxygen concentration, and degassing inefficiencies.

High oxygen concentrations in the deaerator feed water may help promote biological growth conditions and presence. Biological species are observed in the maintenance hole's sludge, underneath maintenance hole gaskets in the deaerator and heat rejection sections of the MSF plant (unit 36). Their presence may be associated with rubber devulcanization and MIC. The presence of bivalve larvae in the deaerator and mature bivalves in unit 21 of the heat rejection section indicates potential issues with the MSF intake travel screens.

In the heat rejection section of the MSF plant (unit 36), galvanic corrosion from incompatible bi-metallic interactions, exacerbated by biofilm, was also observed, and it is suspected that microbes may play a role in MIC. It is concluded that biological fouling of the deaerator packing material and depressurization of the deaerator from maintenance leaks results in degassing inefficiencies leading to high oxygen concentrations within the deaerator system and microbial presence and potential material degradation of gaskets.

It was recommended to:

- Further, investigate the deaerator packing material for biofouling resulting in process declines;
- Change the gaskets of the maintenance holes of the deaerator and heat recovery system to gaskets more resistant to microbial attack and low water absorption;
- Inspect the system thoroughly for leaks with proper routine maintenance;
- Inspect the intake travel screens, process seawater feed lines, and seawater cooling water systems for macro-fouling species and their larvae;
- Inspect and remove corrosion products and repaint maintenance holes (in the heat rejection section) with non-corrosive paints;
- Paint fixing screws with epoxy to reduce bi-metallic galvanic corrosion and follow the recommended bolting torque values to avoid gasket damage.

The observations of algae, iron-oxidizing bacteria, sulfur-reducing bacteria, diatoms, bivalve larvae, and mature bivalves in and near the deaerator units of a large MSF plant are a testament to the tenacity and adaptability of marine life. However, they are also a potentially serious problem to manage, primarily from the abnormally high oxygen levels measured in the units. While the elevated oxygen levels (up to two orders of magnitude above the maximum design limit) have not yet caused extensive corrosion, they have facilitated biofouling and bio-corrosion.

References

[1] A. Eid Al-Rawajfeh, Nanofiltration pretreatment as CO_2 deaerator of desalination feed: CO_2 release reduction in MSF distillers, Desalination, 380 (2016) 12–17.

[2] F. Bodendieck, K. Genthner, Change of Distiller Performance with Fouling, Encyclopaedia of Desalination and Water Resources (DESWARE), UNESCO-EOLSS, Germany, 2008.

[3] R. Sander, Compilation of Henry's law constants (version 4.0) for water as solvent, Atmos. Chem. Phys., 15 (2015) 4399–4981.

[4] D.Á. Simon, D.Z. Pirityi, T. Bárány, Devulcanization of ground tire rubber: microwave and thermomechanical approaches, Sci. Rep., 10 (2020) 16587, doi: 10.1038/s41598-020-73543-w.

[5] A.G. Checa, C. Jiménez-López, A. Rodríguez-Navarro, J.P. Machado, Precipitation of aragonite by calcitic bivalves in Mg-enriched marine waters, Mar. Biol., 150 (2007) 819–827.

[6] K. Kleiber, Body size and metabolism, Hilgardia: J. Agric. Sci., 6 (1932) 315–353.

[7] S.A.L.M. Kooijman, Dynamic Energy and Mass Budgets in Biological Systems, 2nd ed., Cambridge University Press, Cambridge, 2000.

[8] R.H. Peters, The Ecological Implications of Body Size, Cambridge Studies in Ecology, Cambridge University Press, Cambridge, 1983.

[9] X. Hu, Effect of organic alkalinity on seawater buffer capacity: a numerical exploration, Aquat. Geochem., 26 (2020) 161–178.

[10] T.N. Green, N. Hassan, N. Elwaer, C. Fellows, A. Meroufel, A. Al-Mayouf, S. Ali, Characterization and identification of organic molecules in thermal desalination plant scale, Desal. Water Treat., 205 (2020) 12–21.

[11] S.F. Thomas, G.R. McKillop, Substitute materials to replace asbestos in refinery-service gaskets and packings, Oil Gas J., 84 (1986) 21.

[12] H. Al-Haj Ibrahim, A Fundamental Tool for Scientific Computing: Fouling in Heat Exchangers, SCIYO, UNESCO-EOLSS, Germany, 2008, doi: 10.1010/S0017-9310(96)00261-X.

[13] A.M. Shams El Din, M.E. El-Dahshan, R.A. Mohammed, Scale formation in flash chambers of high-temperature MSF distillers, Desalination, 177 (2005) 241–248.

[14] E. Hermann, Marine Biological Materials of Invertebrate Origin, Springer, Cham, ISSN: 2211–0593, 2019, pp. 23–26.

[15] C.M. Fellows, A.A. Al Hamzah, C.P. East, Chapter 21 – Scale Control in Thermal Desalination, Z. Amjad, K.D. Demadis, Eds., Water-Formed Deposits: Fundamentals and Mitigation Strategies, Elsevier, Netherlands, 2021.

[16] M.C. Nash, B.D. Russell, K.R. Dixon, M. Liu, H. Xu, Discovery of the mineral brucite (magnesium hydroxide) in the tropical calcifying alga *Polystrata dura* (Peyssonneliales, Rhodophyta), J. Phycol., 51 (2015) 403–407.

[17] R.F. Schmalz, Brucite in carbonate secreted by the red alga *Goniolithon* sp., Science, 149 (1965) 993–996.

[18] B. Tesson, C. Gaillard, V. Martin-Jézéquel, Brucite formation mediated by the diatom *Phaeodactylum tricornutum*, Mar. Chem., 109 (2008) 60–76.